# Responsive mechanism and coordination mode effect of a bipyridine-based two-photon fluorescent probe for zinc ion*

Han Zhang(张瀚), Zhe Shao(邵哲), and Ke Zhao(赵珂)†

*School of Physics and Electronics, Shandong Normal University, Jinan* 250358, *China*

(Received 7 May 2020; revised manuscript received 2 June 2020; accepted manuscript online 18 June 2020)

The properties of one-photon absorption (OPA), emission and two-photon absorption (TPA) of a bipyridine-based zinc ion probe are investigated employing the density functional theory in combination with response functions. The responsive mechanism and coordination mode effect are explored. The structural fluctuation is illustrated by molecular dynamics simulation. The calculated OPA and emission wavelengths of the probe are consistent with the experimental data. It is found that the red-shift of OPA wavelength and the enhancement of TPA intensity are induced by the increased intramolecular charge transfer mechanism upon metal binding. The structural fluctuation could result in the blue-shift of TPA wavelength and the decrease of the TPA cross section. The TPA properties are quite different among the zinc complexes with different coordination modes. The TPA wavelength of the complexes with two ligands is close to that of the probe, which is in agreement with the experimental observation.

**Keywords:** two-photon absorption, fluorescent probe, zinc ion, coordination mode, bipyridine

**PACS:** 33.20.−t, 42.65.−k, 47.11.Mn, 82.30.Fi **DOI:** 10.1088/1674-1056/aba9b9

## 1. Introduction

In recent years, various kinds of two-photon (TP) fluorescent probes have been developed because of their important applications in TP fluorescence microscopy.[1–4] In comparison with one-photon microscopy, TP fluorescence microscopy could increase penetration depth, lower tissue autofluorescence and self-absorption, and reduce photon-damage and photo-bleaching. Therefore, TP fluorescence microscopy has become a critical tool in imaging of living cells and tissues and TP fluorescent probes has been extensively used to detect cation and anion ions,[5–8] pH values,[9,10] small molecules,[11,12] DNA,[13] and so on. The zinc ion is an important element in living body and takes part in many biological processes.[14–16] To detect the distributions of the zinc ions in the living systems is highly required. A number of turn-on or ratiometric TP probes for zinc ion detection have been synthesized and their bio-imaging applications have been explored.[5–7]

In contrast to plenty of experimental work, the theoretical study on the TP zinc ion probe is still very scarce in the literature.[17–24] Ren and co-workers studied a series of TP zinc ion probes based on the intramolecular charge transfer (ICT)[17–19] and photo-induced electron transfer (PET) mechanism.[20] The natural bond orbital (NBO) analysis was used to explore the ICT mechanism and the characteristics of molecular orbitals were calculated to illustrate the PET mechanism. Bednarska *et al*. elucidated the sensing mechanism for a bipyridine-centered ratiometric zinc ions probe employing the quantum chemical method in combination with molecular dynamics (MD) simulations.[21] The structures of the probe in water were obtained by a force-field MD approach. The average linear and nonlinear optical properties were calculated. In our previous work, the responsive mechanism of several TP zinc ion probes was investigated[22,23] and some new zinc ion probes were designed based on the structure-property relationships.[22] Special emphasis was placed on the effects of isomerism and coordination mode on the optical properties.[24]

Recently, Li *et al*.[25] synthesized a ratiometric TP fluorescence probe for sensing of zinc ions. The two-photon absorption (TPA) cross section of the probe is high and increases after coordination with the $Zn^{2+}$. In order to understand the response mechanism of the probe, we perform a theoretical study on the one-photon absorption (OPA), emission and TPA properties of the probe before and after combination with the $Zn^{2+}$ using density functional theory (DFT). The experiment molecular structures are analyzed by a potential energy surface scan. For a probe in solution at room temperature, the structural fluctuation and coordination mode effect are highly required to take into account. In this work, the structural fluctuation is illustrated by MD simulation and the structure-property relationship is examined. Besides, several coordination modes are considered and the effects on TPA properties are further explored at length. To the best of our knowledge, the coordination mode effects have not been investigated theoretically for TP metal ion sensors by other research groups. Our study will provide a good understanding of the experiment results for TP zinc ion probes.

*Project supported by the Natural Science Foundation of Shandong Province, China (Grant No. ZR2014AM026).

†Corresponding author. E-mail: zhaoke@sdnu.edu.cn

 

## 2. Computational method

In this study, the expressions for one- and two-photon absorption processes are the same as our previous work, such as the ones given in Refs. [22,26]. The TPA cross section can be obtained by calculating the individual TP transition matrix elements[27] and the matrix elements can be calculated through the single residues of the quadratic response function in response theory.[28] The calculation details are as follows. The optimization of ground state geometries is performed by using DFT with the 6-31G(d,p) basis set and the B3LYP hybrid functional. The OPA properties are computed by the time-dependent DFT (TD-DFT) approach at the CAM-B3LYP level with the 6-31G(d) basis set. The first excited state geometry and fluorescence properties are calculated using TD-DFT at the same level. All of the calculations mentioned above are carried out in the Gaussian 16 program.[29] The response theory which is embedded in the Dalton 2013 package[30] is employed for computing the TPA transition matrix and the CAM-B3LYP functional with the 6-31G(d) basis set are used. Moreover, the effect of the methanol solvent is taken into account implicitly using the polarizable continuum model in both Gaussian and Dalton calculations.

In the MD simulations, all of the parameters of molecular force field are taken from the general Amber force field (GAFF)[31,32] in the Amber 14 package.[33] As our previous work,[34,35] the partial atomic charges are obtained by fitting the electrostatic potential from the Hartree-Fock 6-31G(d) calculations for the probe and the solvent molecule. One probe and 1000 methanol molecules are contained in a simulation box. The simulations are performed by the Gromacs[36] program with a time step of 1fs and the Berendsen barostat and thermostat are used.

## 3. Results and discussion

### 3.1. The experiment molecular structure

The chemical structure of the probe, named as A, is shown in Fig. 1. The probe is composed of a dipyridyl center (electron acceptor) and two methyl and benzene end groups (electron donors), which constitute a donor-$\pi$-acceptor-$\pi$-donor type. It has been reported that the probe A has an isomer B where two N atoms are on the same side of the single bond. The AZn and BZn are the corresponding neutral zinc complexes. The optimized geometries of two isomers (A and B) and their zinc complexes (AZn and BZn) are presented in Fig. 2. No imaginary frequency is found in the frequency calculations. The results show that the energy of the B is 4.57 kcal/mol higher than that of the A and the energy of the AZn is 21.13 kcal/mol higher than that of the BZn. The backbones of the A and BZn have good planarity and the two pyridine rings in the center lie practically on the same plane. The related dihedral angles are nearly zero, as shown in Fig. 2. However, the B and AZn have nonplanar structures and the dihedral angles between the two pyridine rings are $-27.6^\circ$ and $6.657^\circ$, respectively. The bond length between the N atom and the $Zn^{2+}$ ion is about 2.1 Å, which is similar to the value in the crystal structure.[37]

The energies of a set of the structures with different dihedral angles between the central two pyridine rings are calculated and the energy curves are shown in Fig. 3. From Fig. 3(a), it can be seen that the energy is the lowest when the dihedral angle is $180^\circ$, as the structure of the A. When the dihedral angle is $100^\circ$, the energy comes to a maximum point. From $180^\circ$ to $100^\circ$, a barrier of 7.79 kcal/mol is needed, which means it is easy to overcome at room temperature. Then, there is a local energy minimum point at around $40^\circ$. Therefore, the A and B can be converted to each other in solution. For the zinc complexes, the case is different. One can see that from the AZn to BZn, as shown in Fig. 3(b), there is nearly no energy barrier, and then the the AZn structure can convert to the BZn directly.

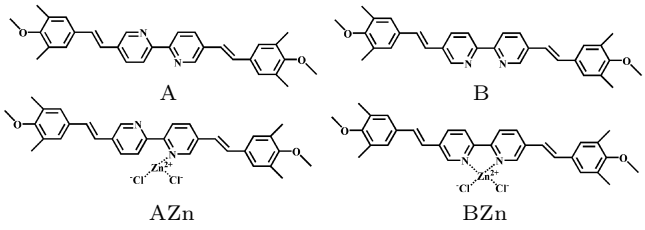


**Fig. 1.** Chemical structures of the molecules (A and B) and their corresponding zinc complexes.

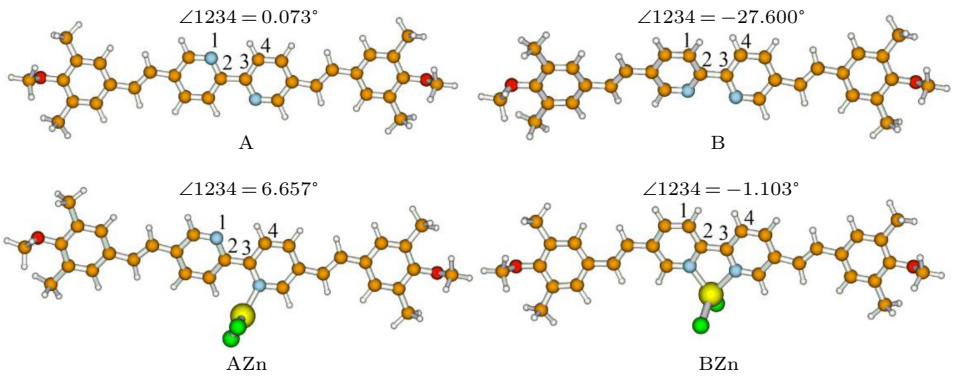


**Fig. 2.** Optimized geometries of the molecules (A and B) and their corresponding zinc complexes.

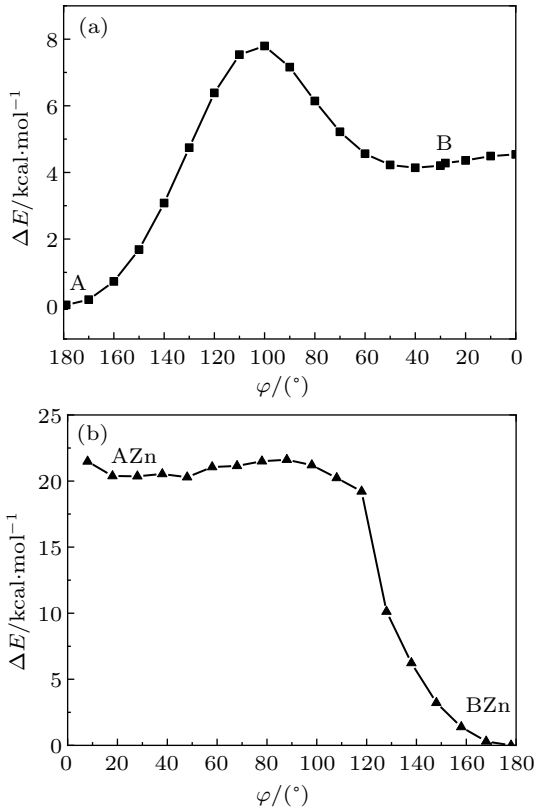


**Fig. 3.** Energy curves from the A to B (a) and from the AZn to BZn (b).

In quantum chemical calculations, the temperature effects usually are not considered. For a molecule in solution at room temperature, the structural fluctuation becomes possible. In some cases, the structural fluctuation could produce important effects on spectra.[35] It is easy to find that the probe A has a very flexible structure because the dihedral angle between the two pyridine rings could be changed. We take the probe A as the initial conformation. Figure 4 gives the evolution of the dihedral angle $\varphi$ during the 2–5 ns MD simulation. One can see that the angle $\varphi$ experiences considerable changes in the range from 180° to 120°. At most of the time, the angle $\varphi$ fluctuated between 180° and 140°. When we take the isomer B as the initial conformation, the isomer B is turned into the probe A very quickly.

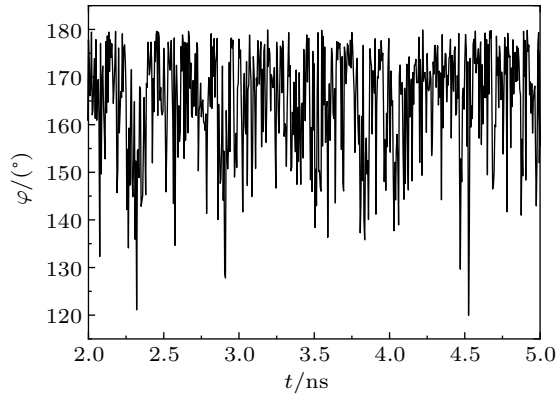


**Fig. 4.** Dihedral angle $\varphi$ during 2–5 ns simulation.

### 3.2. One-photon absorption and emission properties

The experimental linear absorption and emission wavelengths of the probe A are located at around 360 nm and 465 nm. After coordinating with the $Zn^{2+}$ ions, the absorption wavelength shifts to 400 nm and the emission wavelength is observed at 550 nm.[25]

Table 1 gives the calculated OPA wavelength $\lambda_{op}$, oscillator strength $f_{op}$, and transition nature of all the studied molecules. It shows that $\lambda_{op}$ of the probe A is located at 368 nm, which is in good agreement with the value of the experiment. When the molecule binds to zinc ions, $\lambda_{op}$ of the AZn is red-shifted to 381 nm. In comparison with A, $\lambda_{op}$ of the isomer B is blue-shifted a little and the value is 355 nm. This is probably because the isomer B has a nonplanar structure. $\lambda_{op}$ of the BZn is 389 nm, which is also consistent with the experimental observations. One can notice that upon the $Zn^{2+}$ binding, $\lambda_{op}$ of the first excited state has a red-shift for the probes A and B. The red-shifts of the AZn and BZn are equal to 13 nm and 34 nm, respectively. The transition nature shows that the transition between the ground state ($S_0$) and the first excited state ($S_1$) produces the OPA peaks and the transition from the highest occupied molecular orbital (HOMO) to the lowest unoccupied molecular orbital (LUMO) has the most contribution.

The geometry for the first excited state has been optimized by the TD-DFT method at B3LYP level with 6-31G(d,p) basis set in methanol solvent. The obtained fluorescence emission wavelength $\lambda_{em}$, corresponding oscillator strength $f_{em}$, and transition nature are also given in Table 1. $\lambda_{em}$ of the probe A is 462 nm, which is in a good agreement with the value of experiment 465 nm. From free ligand to zinc complex, $\lambda_{em}$ of the AZn is shifted to 486 nm. The difference of emission wavelength between the AZn and A is 24 nm. As for the B and BZn, the difference is larger, and the values come to 32 nm. In comparison with $\lambda_{op}$, $\lambda_{em}$ for all of the molecules are also red-shifted greatly (nearly 100 nm). This large Stokes shift is good for reducing the interference of absorption and emission spectra, thereby improving the sensitivity and accuracy of the detection.

In the experiment of TPA-induced fluorescent, the near-infrared laser is often employed as the excitation source. Its wavelength is near to two times of the OPA wavelength. The TPA-induced fluorescence intensity has a linear dependence on the square of the excitation intensity, which can be used to confirm that the spectra are mainly produced by the TPA process. Although TPA has different selection rules with respect to OPA, the TPA-induced fluorescent process is usually the same as the OPA-induced fluorescent process according to Kasha's rule. The probe we studied is a ratiometric TP probe for zinc ion. For the ratiometric probe, the fluorescence quantum yield usually has considerable values ($> 0.5$) before and after combination with metal ions.

**Table 1.** One-photon absorption and emission properties of the molecules.

| Mol. | $\lambda_{op}$/nm | $f_{op}$ | Transition nature | $\lambda_{em}$/nm | $f_{em}$ | Transition nature |
|---|---|---|---|---|---|---|
| A | 368(360)[a)] | 2.83 | $S_0$–$S_1$ H–L(85%) | 462(465)[a)] | 2.99 | $S_1$–$S_0$ H–L(89%) |
| AZn | 381 | 2.58 | $S_0$–$S_1$ H–L(84%) | 486 | 2.78 | $S_1$–$S_0$ H–L(89%) |
| B | 355 | 2.86 | $S_0$–$S_1$ H–L(85%) | 459 | 3.00 | $S_1$–$S_0$ H–L(85%) |
| BZn | 389(400)[a)] | 2.53 | $S_0$–$S_1$ H–L(87%) | 491(550)[a)] | 2.74 | $S_1$–$S_0$ H–L(85%) |

[a)] from Ref. [25].

### 3.3. Two-photon absorption

The TPA wavelength $\lambda_{tp}$ and cross section $\sigma$ of the six lowest excited states are presented in Table 2. The simulated TPA spectra with Lorentz broadening are illustrated in Fig. 5.

**Table 2.** Two-photon absorption wavelengths $\lambda_{tp}$ and cross sections $\sigma$ of the six lowest excited states of the molecules (A and B) and their corresponding zinc complexes.

| State | A | | AZn | | B | | BZn | |
|---|---|---|---|---|---|---|---|---|
| | $\lambda_{tp}$/nm | $\sigma$/GM | $\lambda_{tp}$/nm | $\sigma$/GM | $\lambda_{tp}$/nm | $\sigma$/GM | $\lambda_{tp}$/nm | $\sigma$/GM |
| $S_1$ | 754 | 1 | 788 | 35 | 725 | 2 | 806 | 9 |
| $S_2$ | 629 | 949 | 656 | 2927 | 625 | 600 | 670 | 3772 |
| $S_3$ | 551 | 0 | 563 | 420 | 546 | 0 | 583 | 996 |
| $S_4$ | 530 | 2077 | 551 | 17 | 526 | 955 | 545 | 2236 |
| $S_5$ | 516 | 26 | 531 | 519 | 515 | 96 | 540 | 30 |
| $S_6$ | 515 | 449 | 528 | 6902 | 514 | 163 | 538 | 20 |

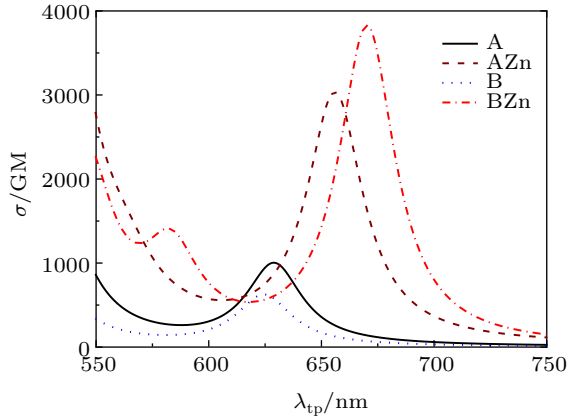


**Fig. 5.** TPA spectra of molecules (A and B) and their corresponding zinc complexes.

For the probe A, the fourth excited state has the largest cross section $\sigma$ with the value of 2077 GM at 530 nm. The second and sixth excited states also have considerable cross sections. The $\sigma$ of the second excited state is 949 GM at 629 nm, which produces one absorption peak in the spectrum (see Fig. 5). When coordinated with the $Zn^{2+}$, the $\sigma$ of the second excited state of the AZn increases up to 2927 GM and the $\lambda_{tp}$ is red-shifted to 656 nm. For the probe B, both second and fourth excited states have large cross sections. The values of $\sigma$ are 600 GM and 955 GM, which are much lower than those of the probe A. This is probably because the isomer B has a torsional structure in comparison with probe A, which is not good for charge transfer. It is well-known that enhancement of intramolecular charge transfer will increase the TPA cross section values of a compound. For the zinc complex BZn, the second and fourth excited states also have strong TPA intensities. The peak position of the BZn is at 670 nm and has a large red-shift of 41 nm with respect to the A. This result is in agreement with the related theoretical research for the similar probe.[19,21] The maximum cross section of the BZn is 3772 GM, which is much higher than that of the A. It is interesting to find that the even states, in most cases, have larger cross sections than those of odd states. It is well known that the two-photon transition obeys different selection rules in comparison with the one-photon transition. The two transition states with the same parity are TPA allowed, but OPA forbidden. The studied molecules have symmetrically substituted donor-$\pi$-acceptor-$\pi$-donor structures. For symmetric molecules, the even states, which have the same parity as the ground state, are TPA allowed states. While the odd states are OPA allowed, but TPA forbidden. So, the even states have larger TP cross sections than those of odd states. In the experiment, the largest TP cross section of the probe was estimated to be 875 GM in the experiment,[25] which is much higher than those common TP fluorescent zinc ion probes.[4] After complexion with the $Zn^{2+}$, the maximum cross section increased to 1350 GM,[25] which is also larger than those common TP fluorophores.[4] Our TPA calculations are consistent with the experimental trend. The calculated largest TPA cross section is also much larger than the TP fluorescent zinc ion probes which were calculated at the same level.[22,24] However, it should be noticed that in our calculations, the TPA wavelength is red-shifted greatly upon the $Zn^{2+}$ binding, while in the experiment, the TPA peaks are nearly at the same wavelength ($\sim$ 700 nm) before and after combination with the $Zn^{2+}$.

As is well known, TPA properties are determined by the ICT process.[17,18,38–40] In order to obtain a better understanding of the ICT process, we have performed calculations of NBO charge analysis for the A and B, as well as their zinc complexes in the ground states and the first excited states. These molecules are divided into three parts $X$, $Y$, and $Z$, as shown in Fig. 6. The net charges of each part are listed in Table 3.

**Table 3.** Net charges (in units of $e$) for divided parts of the molecules in the ground states and the first excited states.

| | $Q_{X0}$ | $Q_{X1}$ | $\Delta Q_X$ | $Q_{Y0}$ | $Q_{Y1}$ | $\Delta Q_Y$ | $Q_{Z0}$ | $Q_{Z1}$ | $\Delta Q_Z$ |
|---|---|---|---|---|---|---|---|---|---|
| A | 0.045 | 0.105 | 0.060 | −0.090 | −0.210 | −0.120 | 0.045 | 0.105 | 0.060 |
| AZn | 0.108 | 0.167 | 0.059 | −0.216 | −0.394 | −0.178 | 0.108 | 0.227 | 0.119 |
| B | 0.046 | 0.109 | 0.063 | −0.093 | −0.216 | −0.123 | 0.047 | 0.107 | 0.060 |
| BZn | 0.090 | 0.220 | 0.130 | −0.178 | −0.460 | −0.282 | 0.088 | 0.238 | 0.150 |

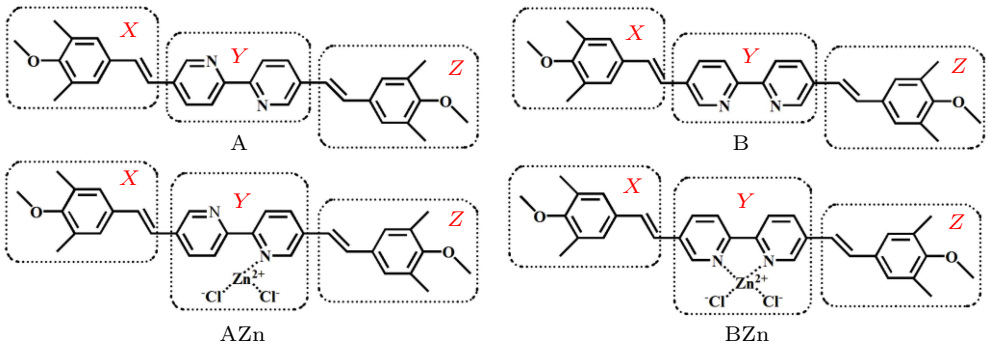


**Fig. 6.** Divided parts of the molecules (A and B) and their corresponding zinc complexes.

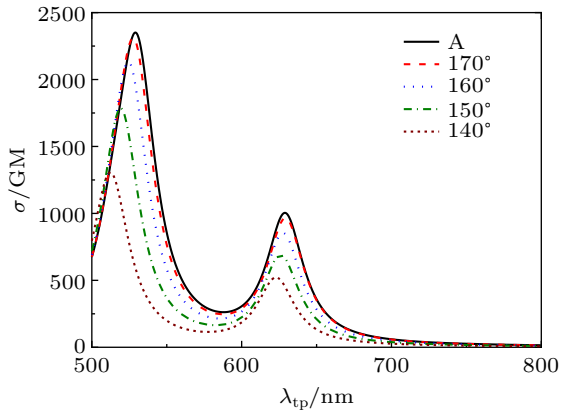


**Fig. 7.** TPA spectra of molecule A and the structures with decreasing dihedral angle.

The $Q_{X0}$ and $Q_{X1}$ stand for the net charge of part $X$ in the ground state and the first excited state, respectively. $\Delta Q_X$ represents the net charge difference of part $X$ between the ground state and the first excited state. Similar to this definition, $\Delta Q_Y$ and $\Delta Q_Z$ denote the net charge difference of part $Y$ and part $Z$ between the ground state and the first excited state. For the probe A, it is found that the net charge of part $X$ in the first excited state $Q_{X1}$ is $0.105e$, which is more electropositive than the value in the ground state $Q_{X0}$, $0.045e$. The net charge of part $Y$ in the first excited state ($Q_{Y1}$, $-0.210e$) is more electronegative than in the ground state ($Q_{Y0}$, $-0.090e$). The case of part $Z$ is the same as part $X$. This indicates that part $X$ and $Z$ are the donors of the molecule and part $Y$ is the acceptor of the molecule. For the AZn, part $X$ and part $Z$ also act as the donors and part $Y$ is the acceptor. But the net charge differences of the two donors are different. Besides, the $\Delta Q_Y$ is $-0.178e$, which means the charge transfer is much larger than that of the A. This demonstrates that the ICT is increased upon metal binding. The charge distribution of the probe B is similar to the case of the A. The $\Delta Q_Y$ of the BZn is $-0.282e$, which means the BZn has the strongest charge transfer ability among these molecules. The ICT is also increased greatly after coordinating with the $Zn^{2+}$ ion.

The structural fluctuation effects are considered and the TPA spectra for the structures with different dihedral angle $\varphi$ based on optimized A conformation are computed and the results are given in Fig. 7. We set the $\varphi$ as 170°, 160°, 150°, and 140°, respectively, which are in the range of fluctuation according to our MD simulations. One can see that the TPA intensity is reduced and the peak position is blue-shifted gradually with the decrease of the $\varphi$. Therefore, it is predicted that the probe A will have broader TPA bands with lower intensities in comparison with the optimized A conformation if the structural fluctuation effect is included.

### 3.4. Coordination mode effect

In the experiment, the TPA peaks are nearly at the same wavelength before and after combination with the $Zn^{2+}$. However, the calculated TPA wavelength of the BZn is red-shifted greatly with respect to the A. Even after considering the structural fluctuation effects, the discrepancy still exists. And also, besides the coordination mode of the AZn and BZn, it is possible that the zinc ion could coordinate with two ligands. Then three new coordination modes AAZn, ABZn and BBZn are taken into account and their structures are shown in Fig. 8. The two ligands are supplied with A or (and) B molecules and the AAZn, ABZn and BBZn have four-, five- and six-coordination geometries, respectively. Due to the steric effects, two A ligands in the AAZn complex have torsional backbone structures. The dihedral angle between the two pyridine rings is about 36°. The bond lengths between the N atoms and the zinc ion are 2.08 Å and 2.10 Å, respectively. In the ABZn complex, the B ligand has a planar center, while the A ligand has a 38° torsional angle between the two pyridine rings. The bond lengths between the N atoms and zinc ion are 2.19 Å, 2.14 Å and 2.12 Å, respectively. As for the BBZn, both two B ligands have planar backbones. The coordination bond lengths are 2.24 Å, 2.16 Å, 2.24 Å and 2.16 Å, respectively. In addition, one can see that the relative orientation of two ligands in the three coordination modes are obviously different. The calculation shows that the energy order of these three complexes is ABZn < BBZn < AAZn.

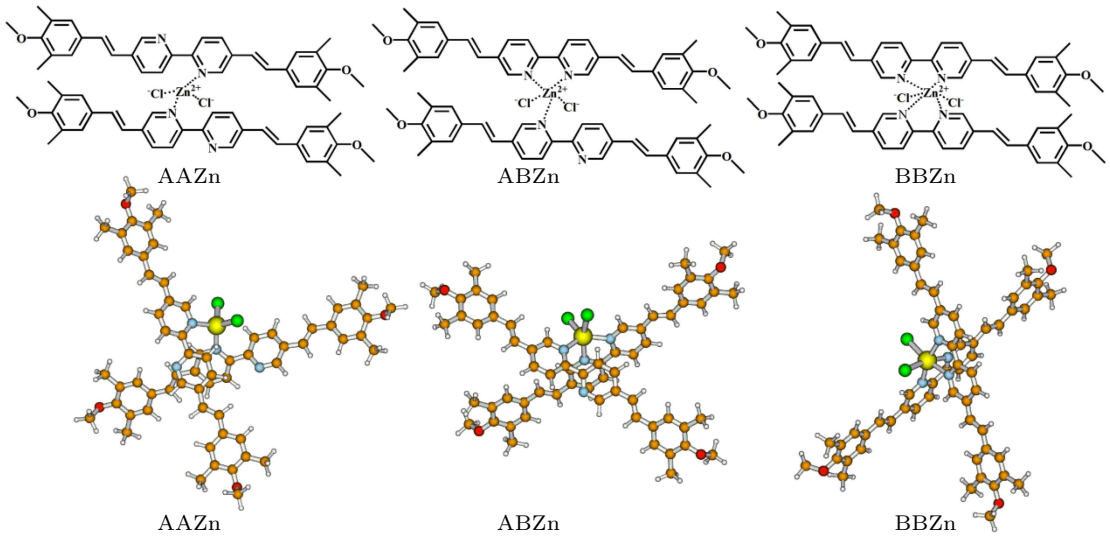


**Fig. 8.** Chemical structures and the corresponding optimized geometries of the zinc complexes AAZn, ABZn, and BBZn.

The TPA wavelength $\lambda_{tp}$ and cross section $\sigma$ of the ten lowest excited states for the three complexes are presented in Table 4. Correspondingly, the simulated TPA spectra with Lorentz broadening are illustrated in Fig. 9. For all of the complexes, the third and fourth excited states have considerable TPA intensity. For the AAZn and BBZn, the $\lambda_{tp}$ of the third and fourth excited states are very close. Therefore, the AAZn has one absorption peak at about 640 nm and the BBZn also has one peak at around 650 nm. While the ABZn has two separated absorption bands at 656 nm and 628 nm. In the lower wavelength range, the seventh and eighth excited states of the AAZn and BBZn are nearly degenerate. Then the AAZn has one absorption peak at 550 nm and the BBZn also has one peak at about 560 nm. But for the ABZn, there are two absorption peaks at around 540 nm and 570 nm produced by several TPA active states. Among the three complexes, the BBZn has the strongest TPA intensity. The peak value comes to 4700 GM at about 650 nm. The TPA intensity of the AAZn or ABZn is much lower than that of the BBZn. The possible reason is both two ligands in the BBZn have planar backbones, which is helpful for charge transfer. It should be noticed that the maximum absorption wavelengths for all of the complexes are located in the vicinity of 650 nm, which is closer to the TPA wavelength of the probe A, 630 nm than those of the AZn and BZn.

**Table 4.** Two-photon absorption wavelengths $\lambda_{tp}$ and cross sections $\sigma$ of the ten lowest excited states of the zinc complexes AAZn, ABZn, and BBZn.

| State | AAZn | | ABZn | | BBZn | |
|---|---|---|---|---|---|---|
| | $\lambda_{tp}$/nm | $\sigma$/GM | $\lambda_{tp}$/nm | $\sigma$/GM | $\lambda_{tp}$/nm | $\sigma$/GM |
| $S_1$ | 745 | 3 | 788 | 6 | 775 | 7 |
| $S_2$ | 736 | 21 | 721 | 18 | 775 | 3 |
| $S_3$ | 647 | 920 | 656 | 2854 | 650 | 1302 |
| $S_4$ | 636 | 1852 | 628 | 1048 | 644 | 3447 |
| $S_5$ | 589 | 44 | 620 | 31 | 601 | 35 |
| $S_6$ | 578 | 36 | 571 | 886 | 601 | 0 |
| $S_7$ | 548 | 358 | 553 | 248 | 559 | 1399 |
| $S_8$ | 548 | 64 | 545 | 14 | 558 | 634 |
| $S_9$ | 530 | 6 | 539 | 562 | 554 | 15 |
| $S_{10}$ | 527 | 27 | 534 | 581 | 549 | 10 |

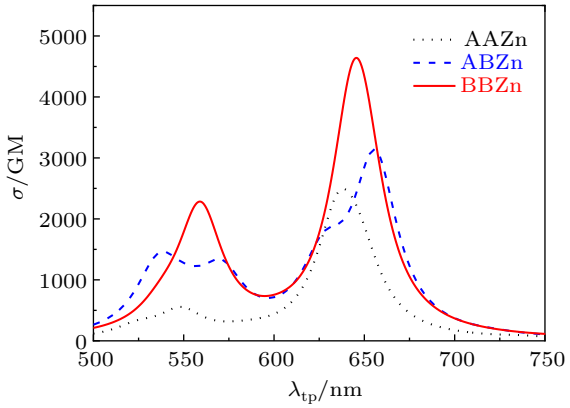


**Fig. 9.** TPA spectra of the zinc complexes AAZn, ABZn, and BBZn.

## 4. Conclusion

The OPA, emission and TPA properties of a bipyridine-based TP fluorescent probe before and after combination with $Zn^{2+}$ are theoretically investigated at a DFT level. The structural fluctuation is illustrated by MD simulations. The ICT mechanism is specified. Several coordination modes are considered and the effects on TPA properties are explored at length. The calculated OPA and emission wavelengths of the probe are consistent with the experimental data. The OPA wavelengths show red-shifts and the TPA cross sections are enhanced greatly due to the increased ICT mechanism upon metal binding. It is found that the structural fluctuation could result in the blue-shift of TPA wavelength and the decrease of TPA intensity. The TPA wavelength and cross section are quite different among the zinc complexes, which demonstrates the

significant coordination mode effects on TPA. It is interesting to find that the TPA wavelengths of the complexes with two ligands are close to that of the probe, which could produce the experimental observations.

## References


[1] Denk W, Strickler J H and Webb W W 1990 *Science* **248** 73
[2] Yao S and Belfield K D 2012 *Eur. J. Org. Chem.* **2012** 3199
[3] Kim D, Ryu H G and Ahn K H 2014 *Org. Biomol. Chem.* **12** 4550
[4] Kim H M and Cho B R 2015 *Chem. Rev.* **115** 5014
[5] Kim H M and Cho B R 2011 *Chem. Asian J.* **6** 58
[6] Sarkar A R, Kang D E, Kim H M and Cho B R 2014 *Inorg. Chem.* **53** 1794
[7] Sumalekshmy S and Fahrni C J 2011 *Chem. Mater.* **23** 483
[8] Kim D, Singha S, Wang T, Seo E, Lee J H, Lee S J, Kim K H and Ahn K H 2012 *Chem. Commun.* **48** 10243
[9] Kim H M, An M J, Hong J H, Jeong B H, Kwon O, Hyon J Y, Hong S C, Lee K J and Cho B R 2008 *Angew. Chem. Int. Ed.* **47** 2231
[10] Kim H J, Heo C H and Kim H M 2013 *J. Am. Chem. Soc.* **135** 17969
[11] Das S K, Lim C S, Yang S Y, Han J H and Cho B R 2012 *Chem. Commun.* **48** 8395
[12] Masanta G, Heo C H, Lim C S, Bae S K, Cho B R and Kim H M 2012 *Chem. Commun.* **48** 3518
[13] Zhang Y, Wang J, Jia P, Yu X, Liu H, Liu X, Zhao N and Huang B 2010 *Org. Biomol. Chem.* **8** 4582
[14] Bush A I, Pettingell W H, Multhaup G, Paradis M D, Vonsattel J P, Gusella J F, Beyreuther K, Masters C L and Tanzi R E 1994 *Science* **265** 1464
[15] Cuajungco M P and Lees G J 1997 *Neurobiol. Dis.* **4** 137
[16] Bush A I and Tanzi R E 2002 *Proc. Natl. Acad. Sci. USA* **99** 7317
[17] Huang S, Zou L Y, Ren A M, Guo J F, Liu X T, Feng J K and Yang B Z 2013 *Inorg. Chem.* **52** 5702
[18] Huang S, Yang B Z and Ren A M 2016 *J. Mol. Struc.* **1114** 65
[19] Wang D, Ren A M, Zou L Y, Guo J F and Huang S 2017 *J. Photoch. Photobio. A* **341** 20
[20] Wang D, Guo J F, Ren A M, Huang S, Zhang L and Feng J K 2014 *J. Phys. Chem. B* **118** 10101
[21] Bednarska J, Zaleśny R, Murugan N A, Bartkowiak W, Ågren H and Odelius M 2016 *J. Phys. Chem. B* **120** 9067
[22] Zhu M Y, Zhao K, Song J and Wang C K 2018 *Chin. Phys. B* **27** 023302
[23] Zhang Y J, Zhang Q Y, Ding H J, Song X N and Wang C K 2015 *Chin. Phys. B* **24** 023301
[24] Zhao K, Song J, Zhu M Y, Zhang H and Wang C K 2018 *Chin. Phys. B* **27** 103301
[25] Li W, Fang B, Jin M and Tian Y 2017 *Anal. Chem.* **89** 2553
[26] Zhao K, Song J and Zhang H 2019 *Acta Phys. Sin.* **68** 183101 (in Chinese)
[27] Luo Y, Norman P, Macak P and Ågren H 2000 *J. Phys. Chem. A* **104** 4718
[28] Olsen J and Jørgensen P 1985 *J. Chem. Phys.* **82** 3235
[29] Frisch M J, Trucks G W, Schlegel H B, *et al.* Gaussian 16, Revision C.01 Gaussian 2016 Inc. Wallingford CT
[30] Aidas K, Angeli C, Bak K L and et al. 2014 *WIREs Comput. Mol. Sci.* **4** 269
[31] Wang J, Wolf R M, Caldwell J W, Kollman P A and Case D A 2004 *J. Comput. Chem.* **25** 1157
[32] Wang J, Wolf R M, Caldwell J W, Kollman P A and Case D A 2005 *J. Comput. Chem.* **26** 114
[33] Case D A, Babin V, Berryman J T, *et al.* 2014 *AMBER 14* (San Francisco: University of California)
[34] Zhao K, Liu P W, Wang C K and Luo Y 2010 *J. Phys. Chem. B* **114** 10814
[35] Zhao K and Luo Y 2010 *J. Phys. Chem. B* **114** 13167
[36] van der Spoel D, Lindahl E and Hess B 2014 *GROMACS User Manual* version 4.6.7, www.gromacs.org
[37] Xue L, Fang Z, Li G and Wang H 2011 *Sens. Actuator B-Chem.* **156** 410
[38] Mu X, Wang J and Sun M 2019 *J. Phys. Chem. C* **123** 14132
[39] Mu X, Wang X, Quan J and Sun M 2020 *J. Phys. Chem. C* **124** 4968
[40] Mu X, Zong H, Zhu L and Sun M 2020 *J. Phys. Chem. C* **124** 2319